Scalings for Droplet Sizes in Shear-Driven Breakup: Non-Microfluidic Ways to Monodisperse Emulsions

V. Cristini[1] **and Y. Renardy**[2]

Abstract: We review studies of a drop of viscous liquid, suspended in another liquid, and undergoing breakup in an impulsively started shear flow. Stokes flow conditions as well as the effects of inertia are reported. They reveal a universal scaling for the fragments, which allows one to use sheared emulsions to produce monodispersity as an alternative to microfluidic devices.

keyword: Drop deformation, drop size distribution, numerical methods.

1 Introduction

Drop breakup is important for a wide range of engineering and biomedical applications including production and processing of emulsions and immiscible polymer blends, aerosols, and drug delivery systems. The application of shear and inertia to a premixed emulsion of various drop sizes is one technique for the production of monodisperse droplets. Experimental, theoretical and numerical studies of drop breakup in imposed flows are reviewed in Rallison (1984); Bentley and Leal (1986); Stone (1994); Basaran (2002); Guido and Greco (2004); Cristini and Tan (2004). Criteria for breakup are investigated experimentally and analytically in, for example, Bentley and Leal (1986); Navot (1999); Blawzdziewicz, Cristini, and Loewenberg (2002, 2003). The distribution of drop fragments resulting from breakup in shear flow is studied in Cristini, Blawzdziewicz, Loewenberg, and Collins (2003); Schmitt, Leal-Calderon, and Bibette (2003), among others. The drop size distribution resulting from breakup events determines the mechanical properties and rheology of such mixtures. These investigations are therefore key to understanding the microstructure of immiscible blend systems in materials processing.

[1] Department of Biomedical Engineering, 3120 Natural Sciences II, University of California, Irvine, CA 92697-2715, USA. E-mail: cristini@math.uci.edu; Fax: 949 824 1727; Tel: 949 824 9132

[2] Department of Mathematics, 460 McBryde Hall, Virginia Tech, Blacksburg, VA 24061-0123, USA. E-mail: renardyy@math.vt.edu

Shear flow is particularly relevant because it is often the dominant flow type in production devices such as extruders and rotor-stator mixers [Bigio, Marks, and Calabrese (1998)]. The study of a single drop in this context contributes to an understanding of the drop size distribution for dilute emulsions in shearing devices.

1.1 Physical Parameters for Stokes Flow

A drop of viscosity μ_d and density ρ_d is suspended in another liquid of viscosity μ_m and density ρ_m. At time $t = 0$, the drop is spherical with radius a. Another option is to place a drop in the liquid that already flows at an imposed constant shear rate $\dot{\gamma}$. For $t > 0$, the ambient fluid undergoes simple shear in the x-z plane with velocity

$$\dot{\mathbf{x}} = \frac{\dot{\gamma}}{2}(\mathbf{S} + \mathbf{A})\mathbf{x}, \ \mathbf{S} = \begin{pmatrix} 0 & 1 \\ 1 & 0 \end{pmatrix}, \ \mathbf{A} = \begin{pmatrix} 0 & 1 \\ -1 & 0 \end{pmatrix}, \quad (1)$$

where $\mathbf{x} = \begin{pmatrix} x \\ z \end{pmatrix}$. The symmetric matrix $\mathbf{S}$ generates elongation along $x = z$ and the antisymmetric matrix $\mathbf{A}$ generates rotation.

We take the densities of the drop and matrix liquids to be the same ($\rho_d = \rho_m$) and focus on the competition between viscous force, capillary force and inertia. The viscosity ratio of the drop to matrix liquids is denoted

$$\lambda = \mu_d / \mu_m . \quad (2)$$

The time scales $\tau_{\dot{\gamma}}$ for drop stretching in the flow, and τ_σ for drop shape relaxation by surface tension are given by

$$\tau_{\dot{\gamma}} = \dot{\gamma}^{-1}, \quad \tau_\sigma = \mu_m a / \sigma. \quad (3)$$

The ratio of these time scales defines the capillary number

$$Ca = \mu_m \dot{\gamma} a / \sigma , \quad (4)$$

where σ is the surface tension.

1.2 Critical Condition for Stokes Flow

Initially, the drop is stretched by viscous shear stress in the external flow. Shear stress is proportional to the viscosity multiplied by the rate of elongation. Continuity of shear stress across the drop/matrix interface therefore yields

$$\lambda \times \{\text{rate of elongation in the drop}\} \sim \{\text{rate of elongation in the matrix}\}. \tag{5}$$

The decomposition (1) for simple shear in the matrix fluid shows that

$$\{\text{rate of elongation in the matrix}\} \sim \{\text{rate of rotation in the matrix}\} \tag{6}$$

In addition, velocity is continuous across the interface; thus,

$$\{\text{rate of rotation in the matrix}\} \sim \{\text{rate of rotation in the drop}\}. \tag{7}$$

Retracing the steps back to (5),

$$\lambda \times \{\text{rate of elongation in the drop}\} \sim \{\text{rate of rotation in the drop}\}. \tag{8}$$

This shows heuristically that when the drop is very viscous ($\lambda \gg 1$), the rate of elongation in the drop is small compared to the rate of rotation in the drop; i.e., the drop can not break. The critical viscosity ratio λ^* beyond which the drop does not break for Stokes flow is roughly 3.

For $\lambda < \lambda^*$, there is a *critical* capillary number, above which the drop breaks [Rallison (1984); Khismatullin, Renardy, and Cristini (2003)]:

$$Ca^* \sim 1. \tag{9}$$

Critical conditions are shown in Fig. 1: $Ca^* \to \infty$ at both $\lambda = 0$ and $\lambda = \lambda^*$. We define a dimensionless time $\bar{t} = t/\tau_{\dot{\gamma}}$, and radius $\bar{a} = a/a^*$, where a^* denotes the radius corresponding to $Ca^* = \mu_m \dot{\gamma} a^*/\sigma$. (9) gives a simple relationship between generated droplet size and imposed flow rate. The larger the flow rate, the smaller the droplet size.

Accurate critical capillary numbers are intrinsically difficult to obtain due to the divergence of the time $\bar{t}_0$ required to reach stationary state [Blawzdziewicz, Cristini,
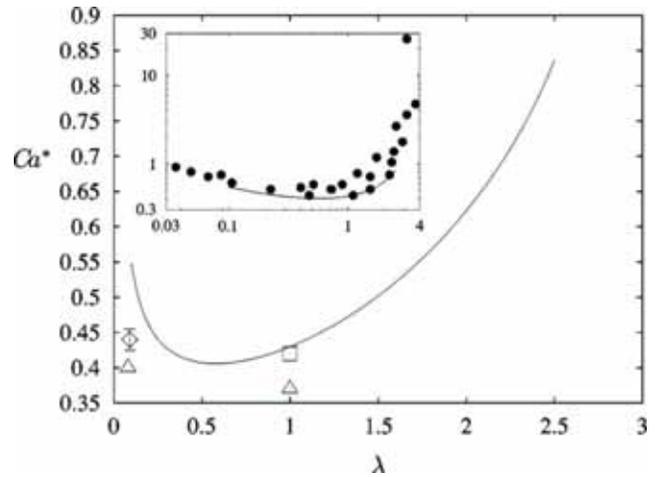
Figure 1 : From Fig. 4 of Cristini, Guido, Alfani, Blawzdziewicz, and Loewenberg (2003). Critical capillary numbers for drops in shear flow from numerical simulations (solid curves), Rallison (1981) (□), Kennedy, Pozrikidis, and Skalak (1994) (△), Janssen (1993) (◇). Inset includes experimental data (●) Grace (1982).

and Loewenberg (2002)],

$$\bar{t}_0 \sim (1-\bar{a})^{-1/2}. \tag{10}$$

Experimental data (inset of Fig. 1) have large scatter due to the uncertainty of determining whether a drop is gradually breaking or gradually attaining a stationary configuration at shear rates close to the critical value. The same difficulty applies to numerical computations.

2 Numerical methods

The two main approaches to simulating drop deformation are interface tracking and interface capturing.

2.1 Interface tracking methods

Interface tracking methods include boundary-integral methods [Pozrikidis (1992); Prosperetti and Oguz (1997); Coulliette and Pozrikidis (1998); Cristini, Blawzdziewicz, and Loewenberg (1998); Zinchenko, Rother, and Davis (1999); Cristini, Blawzdziewicz, and Loewenberg (2001); Hou, Lowengrub, and Shelley (2001); Pozrikidis (2002); Yeo, Matar, de Ortiz, and Hewitt (2003)], finite-element methods [Wilkes, Phillips, and Basaran (1999); Hooper, Cristini, Shakya, Lowengrub, Macosko, and Derby (2001); Hooper, de Almeida,
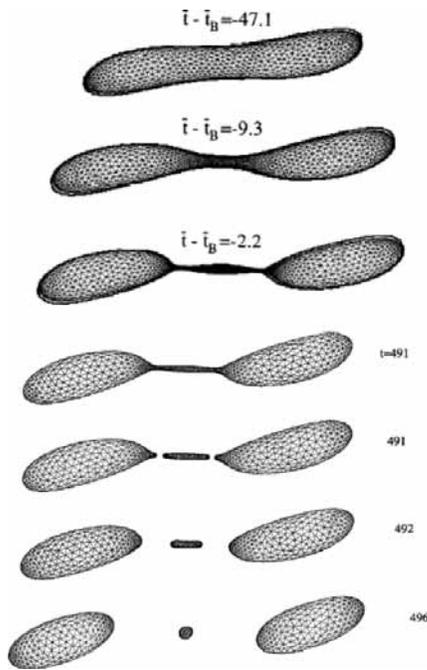
Figure 2 : Adaptive 3-D boundary-integral simulation of drop breakup in shear flow. The simulation is continued past the transition by reconnecting the computational mesh [Cristini, Blawzdziewicz, and Loewenberg (1998, 2001)].

Macosko, and Derby (2001); Notz, Chen, and Basaran (2001)], and immersed-boundary methods [Nobari, Jan, and Tryggvason (1996); Tryggvason, Bunner, Esmaeeli, Juric, Al-Rawahi, Tauber, Han, Nas, and Jan (2001); Shin and Juric (2002); Esmaeeli (2005)]. These are 'sharp-interface' methods; the computational mesh elements lay in part or fully on the fluid/fluid interfaces. Such methods are very accurate for simulating the onset of breakup and coalescence transitions but have difficulties in simulating through and past the transitions.

In boundary-integral methods, the flow equations are mapped from the immiscible fluid domains to the sharp interfaces separating them, thus reducing the dimensionality of the problem (the computational mesh discretizes only the interface). In finite-element methods, the fluid domains are discretized by a volume mesh and thus the dimensionality is not reduced. Both these approaches lead to accurate and efficient solution of the flow equations because the interface is part of the computational mesh and the equations and interface boundary conditions are posed exactly. In immersed-boundary methods,

the interfacial forces are calculated on a surface mesh distinct from the computational volume mesh where the flow equations are solved; thus, in addition, interpolation onto the volume mesh is needed. A three-dimensional boundary integral simulation is shown in Fig. 2. The first three frames show the evolution of a drop towards breakup and the formation of a thinning liquid thread separating two large daughter drops. The labels report the dimensionless time from breakup. The calculated drop shapes (computational mesh) compare well with experimental data (solid contour), demonstrating the high accuracy of the numerical method. These simulations use an adaptive triangulated mesh [Cristini, Blawzdziewicz, and Loewenberg (2001)].

Figure 3 shows an application of the finite-element method to high-Reynolds-number satellite production from a jet [Notz, Chen, and Basaran (2001)]. Cross sections of the computed evolution in time (top) compare well with experimental data (bottom). The computational accuracy allows the authors to recover features of the evolutions such as capillary waves (a-c), overturning of the top and bottom of the satellite in (f), spade-shaped profiles (g, h), and spawning of a subsatellite.
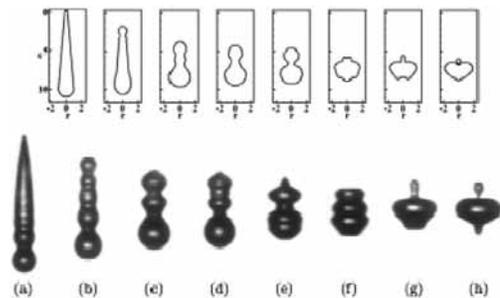
Figure 3 : From Figs. 2 and 3 of Notz, Chen, and Basaran (2001). Finite-element simulation (top) of satellite formation and dynamics from a jet compared to an experiment (bottom).

Near breakup and coalescence transitions, sharp-interface models break down because of the formation of singularities in flow variables [Hou, Lowengrub, and Shelley (1997)], and complex ad hoc cut-and-connect algorithms have been employed [Mansour and Lundgren (1990); Tryggvason, Bunner, Esmaeeli, Juric, Al-Rawahi, Tauber, Han, Nas, and Jan (2001); Cristini, Blawzdziewicz, and Loewenberg (2001)] to change the topology of the meshes and continue simulating through

a transition. A method to automatically reconnect sharp interfaces has been recently developed by Shin and Juric (2002). Nobari, Jan, and Tryggvason (1996) reconnected the interfaces as their separation fell under a prescribed value but noticed that the flow can depend sensitively on the time at which the interface reconnections are performed. Reconnection conditions based on asymptotic theories for liquid thread pinch-off and film drainage are also used to extrapolate to the instant of breakup or coalescence [Keller and Miksis (1983); Eggers and Dupont (1994); Eggers (1995); Blawzdziewicz, Cristini, and Loewenberg (1997); Lister and Stone (1998)]. For instance, the simulation of Fig. 2 (bottom) employs a cut-and-connect mesh algorithm after the asymptotically linear thinning of the liquid thread [Lister and Stone (1998)] has been established. This allows simulations to be continued past the transition while preserving accurate information on breakup time and fragment sizes.

2.2 Interface-capturing methods

Simulations through breakup using interface-capturing methods do not require mesh cut-and-connect operations because the mesh elements do not lay on the interface, but rather the interface evolves through the mesh. Such methods include the lattice-Boltzmann and lattice-gas [Rothman and Zaleski (1997); Chen and Doolen (1998); Nourgaliev, Dinh, Theofanous, and Joseph (2003); Sankaranarayanan, Kevrekidis, Sundaresan, Lu, and Tryggvason (2003); Watanabe and Ebihara (2003)], constrained-interpolation-profile [Yabe, Xiao, and Utsumi (2001)], level-set [Osher and Fedkiw (2001); Jimenez, Sussman, and Ohta (2005); Hogea, Murray, and Sethian (2005)], volume-of-fluid [Scardovelli and Zaleski (1999)], coupled level-set and volume-of-fluid [Sussman and Puckett (2000)] and partial-miscibility-model and phase-field methods [Lowengrub, Goodman, Lee, Longmire, Shelley, and Truskinovsky (1999); Anderson, McFadden, and Wheeler (1998); Yabe, Xiao, and Utsumi (2001); Jacqmin (1999); Badalassi, Ceniceros, and Banerjee (2003); Chen (2002); Yue, Feng, Liu, and Shen (2004, 2005)]. The fluid discontinuities (e.g., density, viscosity) are smoothed and the surface tension force is distributed over a thin layer near the interface to become a volume force (surface tension being the limit as the layer approaches zero thickness). Interface-capturing methods are then ideal for simulating breakup and coalescence in immiscible two-fluid systems (and the ef-

fect of surfactants) and for three or more liquid components, and can be especially powerful for micro channel design. Lattice-Boltzmann methods are based on a particle distribution function and on averaging to capture the macroscopic behavior. The constrained-interpolation-profile, level-set and volume-of-fluid methods describe the macro scale directly and use auxiliary functions advected by the flow (e.g. level-set, volume fraction, and color functions) to mark the different fluid domains.

In Fig. 4, we reproduce a simulation of drop breakup in shear flow using a volume-of-fluid method [Li, Renardy, and Renardy (2000); Renardy, Cristini, and Li (2002); Renardy and Cristini (2001a,b)]. The drop is strongly stretched in the supercritical flow leading to rupture into numerous fragments of alternating sizes (see for comparison, Cristini, Guido, Alfani, Blawzdziewicz, and Loewenberg (2003); Tan, Cristini, and Lee (2006)). The diffuse-interface (phase-field) approach is based on free-energy functionals and uses chemical diffusion in narrow transition layers between the different fluid components as a physical mechanism to smooth flow discontinuities and to yield smooth evolution through breakup and coalescence. The singularity which arises at a pinch-off [Papageorgiou (1995); Eggers (1995); Lister and Stone (1998)] affects the resolution of the subsequent small drops.
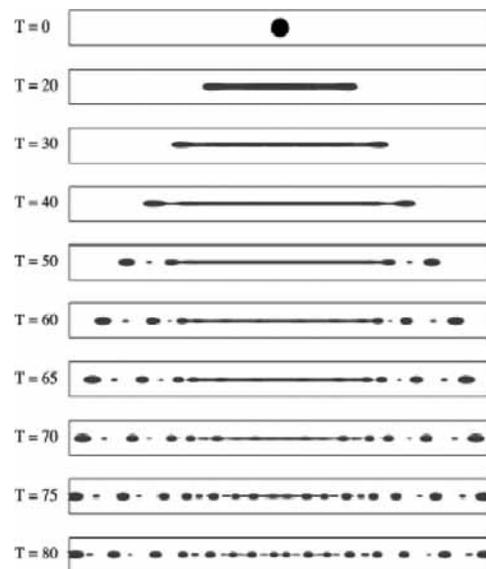
Figure 4 : 3-D volume-of-fluid simulation of drop breakup in simple shear, view along the velocity gradient. Fig. 16 of Li, Renardy, and Renardy (2000).

In Renardy and Renardy (2002), a parabolic reconstruction of the interface in the surface tension (PROST) force for volume-of-fluid methods is formulated. The algorithm achieves convergence with spatial refinements in repeated drop breakup simulations. The main features of PROST are that it reconstructs the interface with a least square fit of a quadratic interface to the values of the volume fraction function for each interface cell, and calculates the curvature directly from the quadratic surface at cell centers. This avoids numerical differentiation of the discontinuous volume fraction function. The PROST algorithm is extended to the Giesekus constitutive law for viscoelastic liquids in Khismatullin, Renardy, and Cristini (2006), where the experimental data of Guido, Simeone, and Greco (2003) are simulated.

Figure 5 (a)-(c) is a breakup simulation for Stokes flow with PROST, and the close agreement with the boundary integral simulation (d) illustrates the accuracy of this sharp-interface volume-of-fluid method.

Figure 6 shows a breakup simulation with inertia. The drop evolves to an ellipsoidal shape, then to a dumbbell with the central portion continuing to stretch and thin. There is vortical motion inside the bulbs which detach to form the first daughter drops. When the mother drop is large enough, the ends of the remaining portion retracts slightly due to surface tension, then bulb up and end-pinching repeats. If the capillary number is sufficiently high, end-pinching leaves behind a long cylindrical thread, where capillary wave breakups are observed. This results in a distribution of large satellite droplets, interspersed with small droplets.

2.3   Adaptive Mesh

Accurate numerical simulations require the computational mesh to resolve both the macro (e.g., droplet size, channel geometry) and micro scales where pinch-off or coalescence occurs; for example, local interface curvature, separation between interfaces, surfactant distributions, and relevant stresses and forces. Adaptive mesh algorithms greatly increase accuracy and computational efficiency in boundary-integral [Cristini, Blawzdziewicz, and Loewenberg (2001)], finite element [Wilkes, Phillips, and Basaran (1999); Hooper, Cristini, Shakya, Lowengrub, Macosko, and Derby (2001); Cristini, Hooper, Macosko, Simeone, and Guido (2002)], immersed boundary [Tryggvason, Bunner, Esmaeeli, Juric, Al-Rawahi, Tauber, Han, Nas, and Jan

(a)

(b)

(c)

(d)
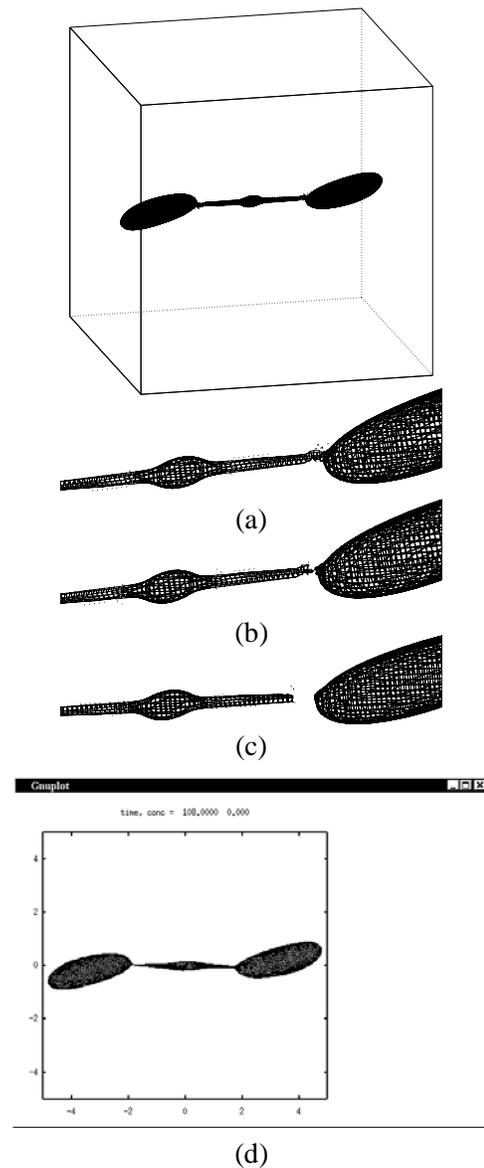
Figure 5 : From Figs. 7-11 of Renardy and Renardy (2002). VOF-PROST simulation (a)-(c). (a) Drop at time 47.7 just before breakup, full view. Lower: view of neck. (b) View of neck at time 47.8 close to breakup. (c) Time 47.9 after breakup. (d) Boundary integral simulation at time 47.5.

(2001)], and interface capturing [Agresar, Linderman, Tryggvason, and Powell (1998); Sussman, Almgren, Bell, Colella, Howell, and Welcome (1999); Provatas, Goldenfeld, and Dantzig (1999); Ubbink and Issa (1999); Ceniceros and Hou (2001); Jeong, Goldenfeld, and
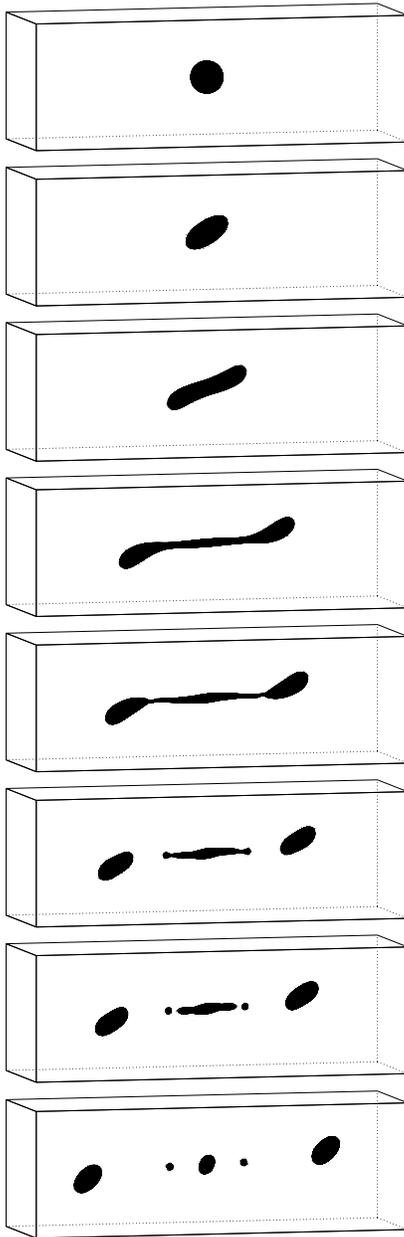
Figure 6 : Numerical simulation of fragmentation. $Re = 12, Ca = 0.175 = 1.14Ca^*, \lambda = 1.$ $t = 0, 1, 9, 19, 21, 22, 22.4, 24.8\dot{\gamma}^{-1}$. The VOF-PROST algorithm is used.

Dantzig (2001); Jeong, Dantzig, and Goldenfeld (2003); Ginzburg and Wittum (2001); Zheng, Roach, and Ismagilov (2003)] methods. Figure 7 shows novel unstructured adaptive meshes in level-set simulations of Anderson,

Zheng, and Cristini (2005); Zheng, Lowengrub, Anderson, and Cristini (2005). Their algorithm automatically imposes a mesh element size proportional to the distance from the interface. As the interfaces deform, approach or pinch-off, the mesh dynamically maintains accurate resolution of the flow near the interface. The 3-D simulation accurately describes drop breakup during retraction of a previously elongated drop.
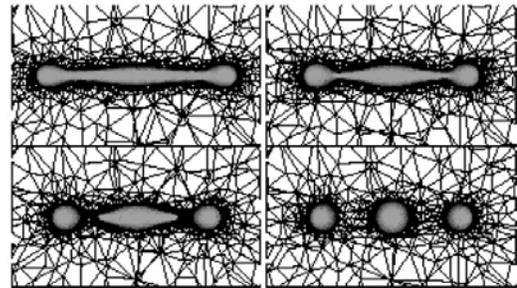
Figure 7 : Adaptive unstructured meshes of tetrahedra maintain computational accuracy during simulations (data from Zheng, Lowengrub, Anderson, and Cristini (2005)). Some tetrahedra may appear skewed as a result of projecting the 3-D mesh onto the plane of the figure.

3   Fragment size distribution for Stokes flow

Fragments may be categorized roughly into three types. The first 'daughters' produced by the primary breakup event have the largest volumes. In Fig. 5, these roughly split the mother drop at criticality. Next comes the neck region between the dumbbells. Capillary force breaks this region into smaller but still substantial 'satellites'; see, for instance, the middle satellite of the last frame of Fig. 6. The third category is comprised of the smallest fragments which lie between the satellites and make up only a few percent of the mother drop volume. Figures 8 and 9 show experimental photographs of fragments produced by breakup in shear. The fragments are found to scale with the critical size a^*, independent of the parent drop radius a_0, so that an appropriate dimensionless daughter radius is $\overline{a_d} = a_d/a^*$. This scaling has also been observed in experiments of drop breakup in shear flow [Marks (1998); Cristini, Guido, Alfani, Blawzdziewicz, and Loewenberg (2003)], and in numerical simulations of drop breakup in stochastic flows [Cristini, Blawzdziewicz, Loewenberg, and

Collins (2003)] and shear flows with inertia [Renardy and Cristini (2001a); Renardy, Cristini, and Li (2002); Renardy and Cristini (2001b)].
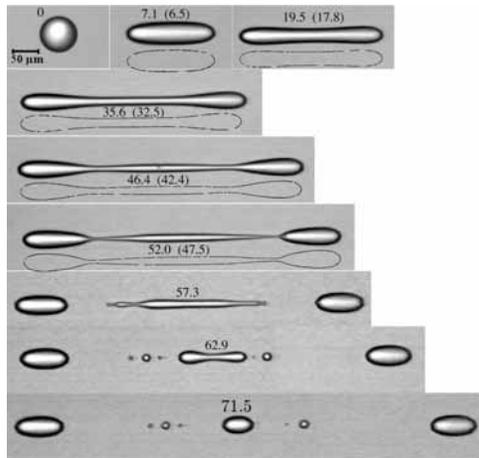
Figure 8 : Fig. 2 of Cristini, Guido, Alfani, Blawzdziewicz, and Loewenberg (2003). Sequence of breaking drop in shear flow $\lambda = 1.02$, $\overline{a} = 1.17$; time $\overline{t}$ as indicated, predicted values shown in parentheses. Images from experiment; profiles from numerical simulation with boundary integral method up to pinch-off event. Top-view of drop, in direction parallel to velocity gradient.

Figure 8 shows a fluid pair with viscosity ratio $\lambda = 1.02$ in Stokes flow just above criticality. Numerical simulations with a boundary integral method are plotted together. In figure 9, the mother drop size is larger so that more droplets are created. The first daughter drops attain a constant value $\overline{a}_d$ for sufficiently super-critical $\overline{a}_0$. In the figures, $\overline{a}_d \sim 0.90$ for $\overline{a}_0 > 1.4$; smaller parent drops have insufficient volume to produce daughters of this size. Experiments at other fluid properties show the same qualitative behavior of daughter drops that saturate to a specific percentage of the critical drop size. After the first daughter drops separate, a 'neck' is left behind which breaks up further, either by end-pinching or capillary-wave instability [Stone and Leal (1989)]. The larger satellite drops scale with the critical size drop, just as in the case of the first daughters. For small satellite drops, the external flow is unimportant. Their sizes are determined by the width of the neck produced by the primary pinch-off event. For $\overline{a}_0 \gg 1$, the neck width is found to scale with a^*. In particular, the dimensionless
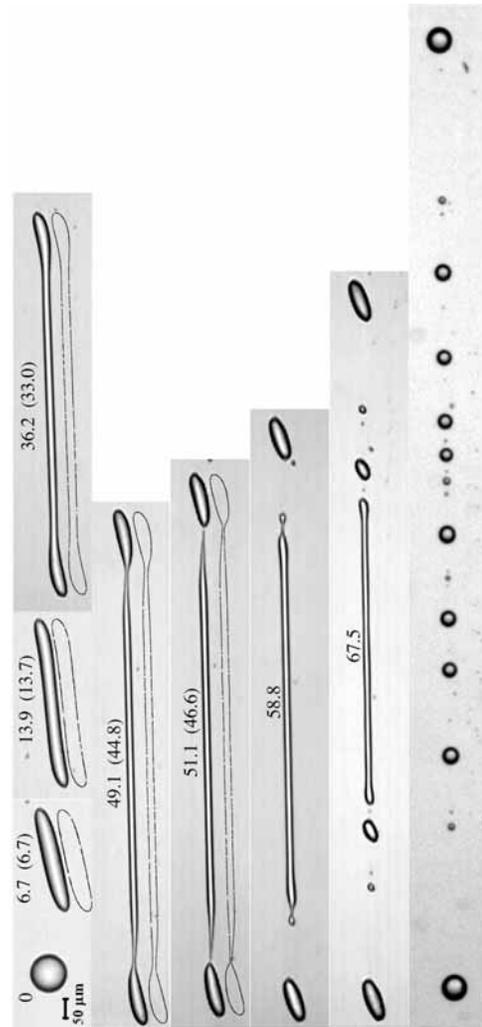
Figure 9 : As in Fig. 8 with $\overline{a} = 1.38$. Side-view of drop, in direction parallel to vorticity. Flow stopped in last frame.

neck length at pinch-off l_n, and equivalent neck radius r_n in Figs. 8 and 9 satisfy

$$\pi r_n^2 l_n = \overline{v}_0 - 2\overline{v}_d, \tag{11}$$

where $\overline{v}_0 - 2\overline{v}_d$ is the excess volume of the parent drop. For large $\overline{a}_0$, r_n approaches a fixed value, and satellites produced by the breakup of the neck therefore scale with the critical drop size a^*. Thus, all drop fragments scale with the critical drop size.

Cumulative size distributions of drop fragments obtained from Stokes flow experiments are shown in Fig. 10 [Cristini, Guido, Alfani, Blawzdziewicz, and Loewenberg (2003)]. The vertical axis shows the fraction of

daughter drops of size less than or equal to the number plotted on the horizontal axis. The distributions for each experiment show two distinct daughter drops and three size classes of satellite drops (1) $0.4 < \overline{a} < 0.8$, (2) $0.10 \leq \overline{a} \leq 0.3$, and (3) $\overline{a} \leq 0.1$. The number of satellites within each class is denoted by $N_i(i = 1, 2, 3)$. The largest (class 1) satellites are clearly distinguishable. The number of class 1 and 2 satellites are approximately equal, consistent with the alternating periodic sequence of large and small satellites that is typical of jet breakup. Accordingly, class 2 satellites are defined as the N_2 largest subclass-1 fragments, where $N_2 = N_1 + 1$. The smallest (class 3) fragments account for only $\approx 0.1\%$ of the parent drop volume. Figure 11 replots the same information as Fig. 10, but shows separately the cumulative distribution of the primary daughter drops and the class 1 and 2 satellites. For large $\overline{a_0}$, the distribution of large satellites shows a tendency to become independent of the parent drop size, consistent with the scaling arguments discussed earlier. Zhao and Goveas (2001) observed that a narrower size distribution of fragments is produced by drop breakup in viscoelastic, rather than Newtonian fluids.

Methods for producing controlled micro-sized droplets mostly rely on the use of surfactants and complex fluids in a variety of flows such as shear (see section 5 below), co-flowing streams [Umbanhowar, Prasad, and Weitz (2000)] and extrusion flow [Kobayashi, Yasuno, Iwamoto, Shono, Satoh, and Nakajima (2002)]. Even without the use of surfactants, Cristini, Guido, Alfani, Blawzdziewicz, and Loewenberg (2003) demonstrated that nearly bi-disperse emulsions of large numbers of microscopic droplets of controlled sizes and generation times can be achieved; see Figs. 10 and 11. The two sizes alternate, perhaps because of the asymmetrical evolution of the drop interface near the pinch-off region into cones with different angles during the final stages of pinch-off [Lister and Stone (1998)].

The scaling for the first daughter drops and neck fragments aid in interpreting the experimental data of Section 4.6 of Marks (1998). His Fig. 4.6.1.a, reproduced in Fig. 12 gives five sample histograms of daughter drop sizes, placed in four bins. The 1.0 bin, 0.75 bin, 0.50 bin and 0.25 bin represent $0.75 < Ca_d/Ca^*$, $0.50 < Ca_d/Ca^* < 0.75$, $0.25 < Ca_d/Ca^* < 0.50$, $Ca_d/Ca^* < 0.25$, respectively. The first daughter drops fall into the 1.0 bin. The neck fragments mostly fall into the 0.75
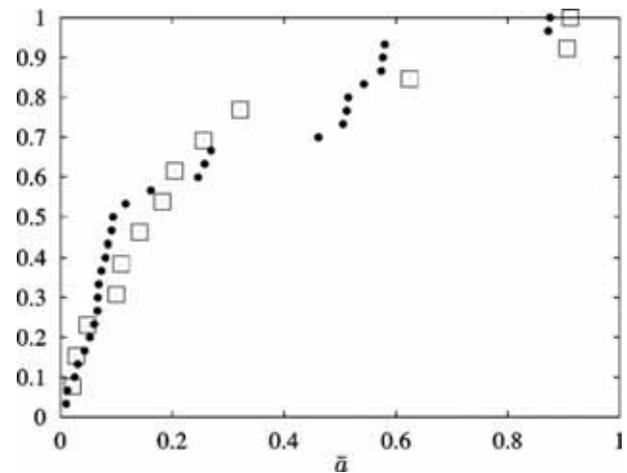
Figure 10 : Fig. 10 of Cristini, Guido, Alfani, Blawzdziewicz, and Loewenberg (2003). Cumulative size distribution of drop fragments from experiments; $\lambda = 1.02$, $\overline{a}_0 = 1.22$ ($\square$), $\overline{a}_0 = 1.38$ ($\bullet$).
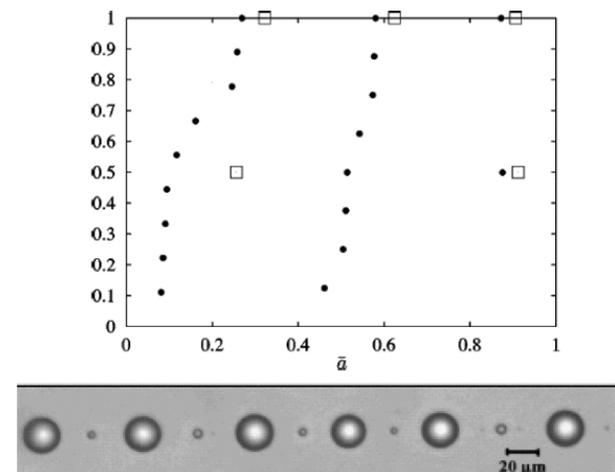
Figure 11 : Generation of nearly bi-dispersed emulsion (From Figs. 11 and 12 of Cristini, Guido, Alfani, Blawzdziewicz, and Loewenberg (2003)). The cumulative distribution of droplets of alternating sizes (inset) formed from breakup of a mother drop in shear flow is shown. The droplet sizes $\overline{a}$ are rescaled with the maximum stable size in the flow.

bin, while tiny drops fall into the other two bins. Beyond the production of the two largest daughters, no other drops of this order of magnitude are produced because the rest of the drops come from the elongated neck. The trend, therefore, is that as the mother capillary number
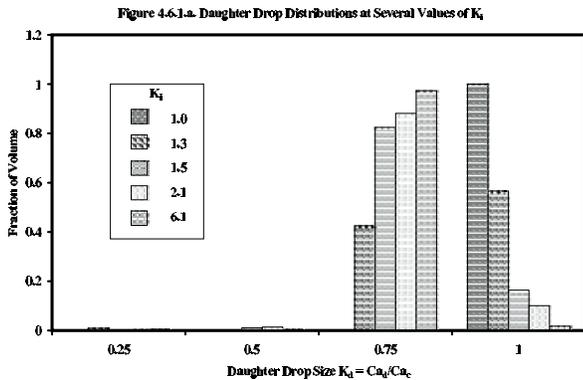
Figure 12 : Fig. 4.6.1.a of Marks (1998). Daughter drop size distributions at several values of $K_i = Ca/Ca^*$. The horizontal axis is daughter drop size $K_d = Ca_d/Ca^*$. Five sample histograms at various values of K_i are shown. These graphs represent typical histograms and were chosen to show a range of K_i's.

increases, the volume fraction in the 0.75 bin increases and eventually dominates. The histogram at $K_i = 1.0$ denotes the fact that just above criticality, most of the drop goes into the first daughter drops in the 1.0 bin. Our results suggest that just two daughter drops fall into the 1.0 bin and the neck fragments fall into the 0.75 bin. The moons fall into the smaller bins. We predict from this that when $K_i = Ca/Ca^* = 2$, the volume fraction of the neck is 0.86, and when $K_i = 6.1$, it is 0.995. This is a close prediction of the two histograms in his figure. Generally, at sufficiently super critical conditions, the total number of main fragments N are expected to scale as

$$N \sim (k/\alpha)^3, \tag{12}$$

where $k = Ca/Ca^*$ and α is the fragment radius/critical radius. This scaling is obtained from conservation of volume.

4   Inertia-induced breakup

Inertia is measured by the Reynolds number

$$Re = \rho_m \dot{\gamma} a^2 / \mu_m . \tag{13}$$

There are three trends for the overall effect of inertia [Li, Renardy, and Renardy (2000); Renardy and Cristini

(2001a)]. First, inertia rotates the drop, so that at higher Reynolds numbers, the steady states are more aligned toward the vertical than in Stokes flow and therefore the drop experiences greater shear. Secondly, in Stokes flow, the flow inside the drop consists of a single vortical swirl. With increased inertia, the velocity field bifurcates, with additional swirls. Thirdly, the length of the drop in steady states just below breakup shortens as inertia increases. The symmetry across the mid-plane of the steady state, evident in Stokes flow, is lost.

For large Reynolds numbers, the Reynolds stress is of order $\rho|\mathbf{v}|^2$ where the speed is $\dot{\gamma}a$. When this inertial stress reaches the magnitude of capillary stress, which is of order σ/a, the drop breaks: $\rho\dot{\gamma}^2 a^2 \sim \sigma/a$. Division by $\mu\dot{\gamma}$ yields the order of magnitude of the critical Reynolds number, above which the drop breaks:

$$Re \sim 1/Ca. \tag{14}$$

In fact, the ratio of inertial to capillary forces is the Weber number

$$We = ReCa. \tag{15}$$

In the inviscid limit, the critical Weber number is approximately 3.3, which is consistent with the scaling of (14).

Renardy and Cristini (2001b) and Renardy, Cristini, and Li (2002) focuss on the case of equal viscosities and densities for the drop and matrix liquids, and investigate neck breakup by keeping the flow strength the same and increasing the parent drop size. For example, when fluid properties and external flow are fixed at $Re = 391Ca^2$, the first daughter drops are approximately 50% to 60% of the critical drop volume. The volumes of the neck drops are 10% to 15% of the critical drop volume. The moons which are spawned from the neck immediately after the first daughter drops detach are extremely small. As the capillary number increases, more of the volume goes into the neck and its breakup approaches that of a filament. Figure 13 shows evolution at $Re = 15, Ca = 0.196 = 1.27Ca^*$, where the first daughter drop volume is 54% of the critical volume. The volumes of the main neck fragments again lie between 10% to 17% of the critical drop volume. Each main drop is followed by one or more small drops, or 'moons'.

Figure 14 shows mother drops indicated by circles. The first daughter drops (indicated by stars) approach 54% of the critical volume (radius $a_d \approx 0.81a^*$) as the mother
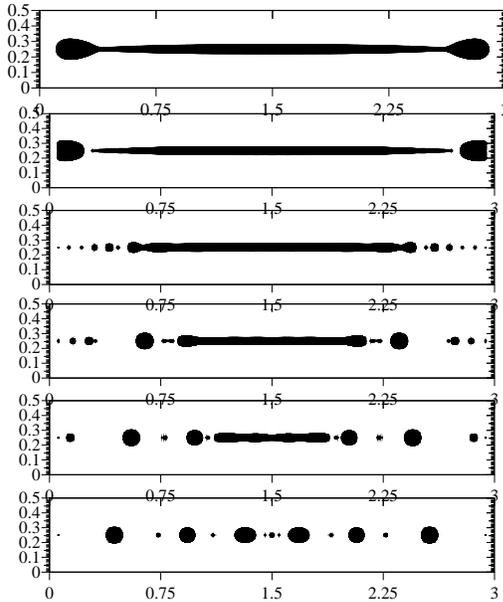
Figure 13 : Fig. 11 of Renardy, Cristini, and Li (2002). $Re = 15, Ca = 0.196 = 1.27Ca^*$, top view, Breakup sequence computed with VOF-CSF.
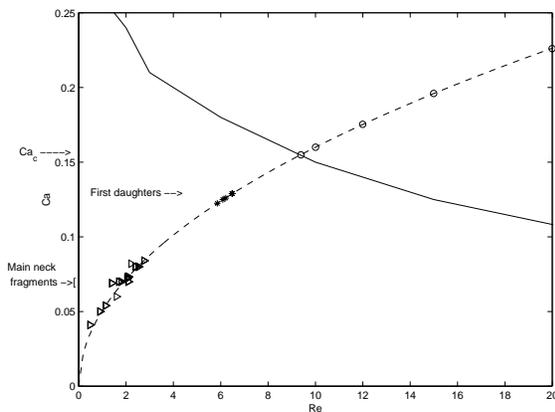
Figure 14 : Fig. 12 of Renardy, Cristini, and Li (2002). *Re* vs *Ca* for the critical curve (solid); $Re = K.Ca^2$ (dashed), $K = 391$, follows an experiment with fluid properties and flow strength fixed, while the radius of mother drop varies. Circles represent mother drop data. Asterisks denote first daughter drop data Re_d vs Ca_d. Triangles denote the rest of the fragments. Small fragments at the level of the discretized mesh are not included.

drop size increases. Compared with Stokes flow results discussed in section 3 (roughly 70% of volume, corresponding to $a_d \approx 0.9a^*$), the drops are smaller with inertia. The fragments from the neck (Δ) lie between 10% to 17% of the critical volume (radius $\approx 0.5a^*$, to be contrasted to the value $0.64a^*$ found by Cristini, Guido, Alfani, Blawzdziewicz, and Loewenberg (2003) from experiments for drop-to-matrix viscosity ratio 0.1). Smaller fragments with $a_d/a_0 < 0.3$ occur in each numerical simulation and are not included in the plot because their volume fraction is small. These results indicate that the size of the large satellites produced from breakup events in the slender neck also scales at large capillary numbers with the critical size.

For sufficiently high capillary number (mother drop size), we find that the main contribution to the volume distribution resulting from the neck lies in the range $0.4 < Ca_d/Ca^* < 0.6$. These drops are slightly smaller than for Stokes flow, for which experimental data in Section 4.6 of Marks (1998) put these in the range $0.5 < Ca_d/Ca^* < 0.75$. These Stokes flow results and the present work conclude that there are tiny drops that contribute relatively little volume fraction for $Ca_d/Ca^* < 0.4$.

At the instant when the first daughter drops pinch off, the neck is elongated to roughly its maximum length, and cylindrical in a central region, tapering off to pencil tips toward the ends. Renardy, Cristini, and Li (2002) tabulates the 'effective' capillary number for the cylindrical neck Ca_n. This is calculated from the length L of the neck (projected onto the x-axis) just after the first daughter drops detach, and the volume in the neck. An effective radius r_n is calculated for this, assuming the neck is cylindrical, and of length L, or $\pi r_n^2 L = (4/3)\pi a_0^3 - 2(4/3)\pi a_d^3$, so that

$$r_n = \left[\frac{4a_0^3(1 - 2(\frac{a_d}{a_0})^3)}{3L}\right]^{1/2}, \tag{16}$$

where a_d is the first daughter drop radius, and

$$Ca_n = Ca(r_n/a_0). \tag{17}$$

At $Re = 15$, the drops which result from the neck have capillary numbers Ca_{Dneck} between 0.08 and 0.09, and if $Ca_{Dneck} = FCa_n$, then F ranges from 2.4 to 2.8. If the breakup were a capillary breakup of a viscous jet in a quiescent liquid as considered in Tjahjadi, Stone, and Ottino (1992), then

$$Ca_{Dneck} = FCa_n, \quad F = 2. \tag{18}$$

Here, however, we have repeated end-pinching, which produces larger drops.

Figure 15 shows the volume fraction relative to the mother drop volume, $V_d/V_a = (Ca_d/Ca^*)^3/(Ca_a/Ca^*)^3$, for each Ca_d/Ca^*. There are always tiny drops between the main fragments which have not been included in the graphs. The trend, as the mother drop size increases, is the growth in drops of size roughly half that of the mother drop. The first daughter drops remain as the largest drops, at roughly 0.8 of the mother drop volume, and there are no other drops of that magnitude in the simulations reported.

The scaling for the drops As the capillary number increases along the parabola shown in Fig. 14, the first daughters saturate to a specific percentage of the critical drop size. The neck radius determines the size of the subsequent drops because they are of the same order of magnitude. As the capillary number increases to infinity, the ratio of daughter drop radii to mother drop radius decreases to zero, $a_d/a_0 \to 0$ and equation (16) shows that the effective neck radius satisfies

$$r_n \sim L^{-1/2} a_0^{3/2}. \tag{19}$$

The capillary numbers covered in Renardy, Cristini, and Li (2002) are not sufficiently large for this scaling to apply, because the ratio a_d/a_0 is not negligible. Therefore, in our regime, r_n is influenced by the two competing effects in equation (16): L increases with increasing Ca, and the numerator $1 - 2(a_d/a_0)^3$ also increases.

For large capillary numbers, the effect of surface tension is initially small and the drop stretches following the simple shear flow, elongates, until eventually, the cross-section of the drop evolves to a circular shape, length scales are reached at which surface tension becomes important, and pinching begins. This pinching begins when an effective radius is approximately the critical radius:

$$r_e \approx r_c, \qquad r_c = a_0 \frac{Ca^*}{Ca}. \tag{20}$$

This effective radius might be interpreted either as the effective neck radius for an extremely elongated case,

but more appropriately for our simulations, as an average radius for a less elongated shape, where $\pi r_e^2 L_T$ equals the original drop volume, with L_T being the total length. When pinch-off occurs, the total length of the drop is of order

$$L_T \sim r_c^{-2} a_0^3 \sim a_0 (\frac{Ca}{Ca^*})^2. \tag{21}$$

(a)

(b)

(c)
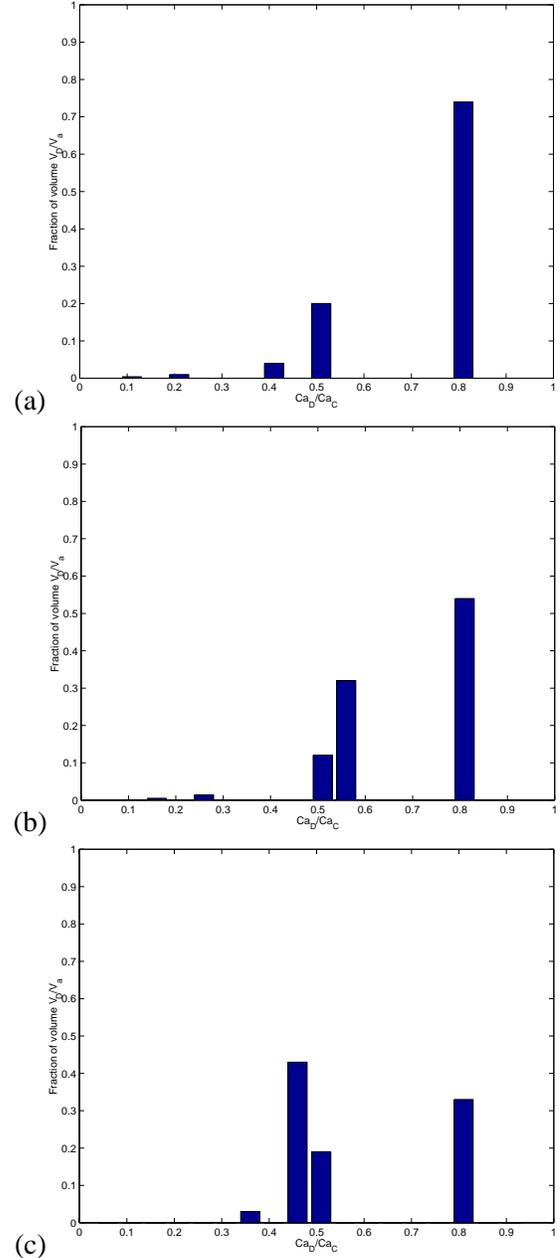
Figure 15 : Fig. 17 of Renardy, Cristini, and Li (2002). Drop size distribution. (a) $Re = 12$, $Ca = 0.14Ca^*$. (b) $Re = 15, Ca = 1.27Ca^*$. (c) $Re = 20, Ca = 1.47Ca^*$. This excludes moons which lie between every main drop and account for a few percentage of the mother drop size.

Note that along the parabola of Fig. 14, $Re = K.Ca^2$, and equation (21) gives

$$L_T \sim Re. \tag{22}$$

5 Complex Fluids

Emulsification is typically promoted by surfactants which decrease surface tension on the droplet interfaces [Stone and Leal (1990); Milliken, Stone, and Leal (1993); Milliken and Leal (1994); Pawar and Stebe (1996); Eggleton, Pawar, and Stebe (1999); Li and Pozrikidis (1997); Siegel (1999); Maldarelli and Huang (1996)]. Monodispersed emulsions of large numbers of droplets with controlled sizes are generated using the tip-streaming phenomenon due to redistribution of surfactants to localized end caps on the drop interface [Bruijn (1993); Eggleton, Tsai, and Stebe (2001)].

Experimental studies show that the use of complex fluids can lead to a dramatic alteration of the rupturing phenomenon Utracki and Shi (1992). Mason, Bibette, and Weitz (1996); Mason and Bibette (1997) produced monodisperse emulsions in a narrow-gap shear cell with a viscoelastic medium; Fig. 16 shows their size distribution.
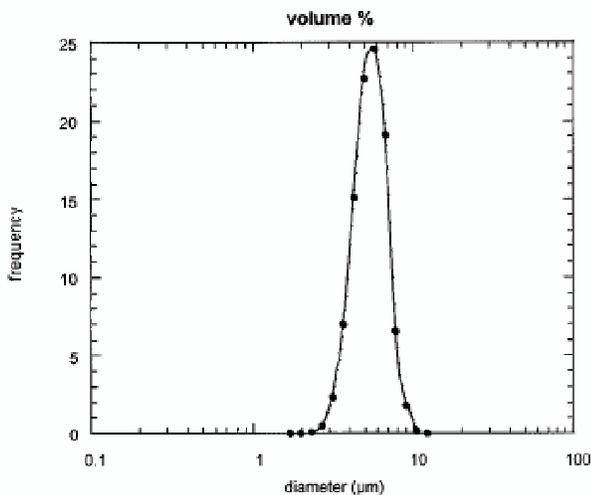
Figure 16 : Fig. 8 of Mabille, Schmitt, Gorria, Calderon, Faye, Deminiére, and Bibette (2000). Size distribution of an emulsion obtained by shearing at 2500 s^{-1}, a premixed emulsion whose elasticity is mainly provided by the continuous phase: $C = 30\%; \Psi = 40\%; D[4,3] = 5.5\mu m; U = 19.3\%$.

Zhao and Goveas (2001) study a dispersed Newtonian phase in a Newtonian medium and a viscoelastic medium under the same shear rates. Initially, the emulsion contains mother drops of various sizes. During satellite formation, the viscoelastic medium produces cylinders of more uniform radii than the Newtonian medium. The cylinders break up due to capillary waves and result in more uniform daughter drops; see Fig. 17.
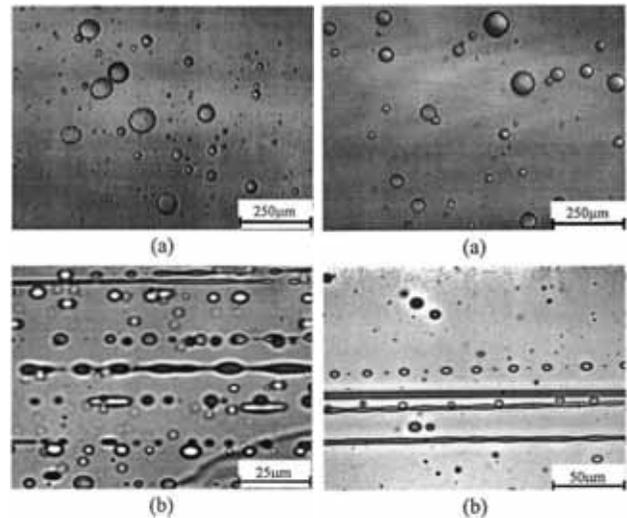
Figure 17 : From Figs. 3 and 4 of Zhao and Goveas (2001). Left: (a) Presheared Newtonian emulsion containing 2 wt % silicone oil in glycerol with 2 wt % TWEEN-80, which corresponds to a viscosity ratio of 0.453. (b) Newtonian emulsion under shear. Drops of different sizes are deformed into cylinders which have different widths at breakup. The resulting daughter drops are nonuniform along the length of the cylinder. Right: (a) Presheared viscoelastic emulsion containing 2 wt % silicone oil in an aqueous solution of 12 wt % PVP and 2 wt % SDS, which corresponds to a viscosity ratio of 0.482. (b) Viscoelastic emulsion under shear, showing that cylinders have similar widths at breakup. The resulting daughter drops are very uniform.

6 Conclusions

Theoretical, numerical and experimental investigations of drop breakup in sheared emulsions were reviewed. The magnitude of flow and fluid properties are important in determining the drop size distribution. The examination of universal scalings for this type of flow leads

to the idea that sheared emulsions can be used as an alternative to microfluidics for the production of controlled monodisperse droplets. Drop sizes can be optimized with the use of direct numerical simulations. Open challenges to be addressed include the study of the effect of complex fluids such as viscoelastic liquids to achieve desired drop sizes. Finally, for non-dilute emulsions, effects of coalescence events need to be taken into account [Lappa (2005a,b)].

References

Agresar, G.; Linderman, J. J.; Tryggvason, G.; Powell, K. G. (1998): An adaptive cartesian front-tracking method for the motion, deformation and adhesion of circulating cells. *J. Comp. Phys.*, vol. 143, pp. 346–380.

Anderson, A.; Zheng, X.; Cristini, V. (2005): Adaptive unstructured volume remeshing - I: The method. *J. Comp. Phys.*, vol. 208, pp. 616–625.

Anderson, D. M.; McFadden, G. B.; Wheeler, A. A. (1998): Diffuse-interface methods in fluid mechanics. *Ann. Rev. Fluid Mech.*, vol. 30, pp. 139–166.

Badalassi, V.; Ceniceros, H.; Banerjee, S. (2003): Computation of multiphase systems with phase field models. *J. Comp. Phys.*, vol. 190, pp. 371–397.

Basaran, O. A. (2002): Small-scale free surface flows with breakup: Drop formation and emerging applications. *AIChE J.*, vol. 48(9), pp. 1842–1848.

Bentley, B. J.; Leal, L. G. (1986): An experimental investigation of drop deformation and breakup in steady, two-dimensional linear flows. *J. Fluid Mech.*, vol. 167, pp. 241–83.

Bigio, D. I.; Marks, C. R.; Calabrese, R. V. (1998): Predicting drop breakup in complex flows from model flow experiments. *International Polymer Processing*, vol. XIII2, pp. 192–198.

Blawzdziewicz, J.; Cristini, V.; Loewenberg, M. (1997): Aanalysis of drop breakup in creeping flows. *Bull. Am.Phys. Soc.*, vol. 42, pp. 2125.

Blawzdziewicz, J.; Cristini, V.; Loewenberg, M. (2002): Critical behavior of drops in linear flows: I. phenomenological theory for drop dynamics near critical stationary states. *Phys. fluids*, vol. 14 (8), pp. 2709–2718.

Blawzdziewicz, J.; Cristini, V.; Loewenberg, M. (2003): Multiple stationary states for deformable drops in linear stokes flows. *Phys. Fluids*, vol. 15, pp. L37–L40.

Bruijn, R. A. D. (1993): Tipstreaming of drops in simple shear flows. *Chem. Eng. Scie.*, vol. 48, pp. 277–284.

Ceniceros, H.; Hou, T. (2001): An efficient dynamically adaptive mesh for potentially singular solutions. *J. Comp. Phys.*, vol. 172, pp. 609–639.

Chen, L. (2002): Phase field models of microstructure evolution. *Annu. Rev. Mat. Res.*, vol. 32, pp. 113–140.

Chen, S.; Doolen, G. D. (1998): Lattice Boltzmann method for fluid flows. *Annu. Rev. Fluid Mech.*, vol. 30, pp. 329–364.

Coulliette, C.; Pozrikidis, C. (1998): Motion of an array of drops through a cylindrical tube. *J. Fluid Mech*, vol. 358, pp. 1–28.

Cristini, V.; Blawzdziewicz, J.; Loewenberg, M. (1998): Drop breakup in three-dimensional viscous flows. *Phys. fluids*, vol. 10(8), pp. 1781–1783.

Cristini, V.; Blawzdziewicz, J.; Loewenberg, M. (2001): An adaptive mesh algorithm for evolving surfaces: simulations of drop breakup and coalescence. *J. Comp. Phys.*, vol. 168, pp. 445–463.

Cristini, V.; Blawzdziewicz, J.; Loewenberg, M.; Collins, L. (2003): Breakup in stochastic Stokes flows: Sub-Kolmogorov drops in isotropic turbulence. *J. Fluid Mech.*, vol. 492, pp. 231–250.

Cristini, V.; Guido, S.; Alfani, A.; Blawzdziewicz, J.; Loewenberg, M. (2003): Drop breakup and fragment size distribution in shear flow. *J. Rheol.*, vol. 47(5), pp. 1283–1298.

Cristini, V.; Hooper, R. W.; Macosko, C. W.; Simeone, M.; Guido, S. (2002): A numerical and experimental investigation of lamellar blend morphologies. *Ind. Eng. Chem. Res.*, vol. 41, pp. 6305–6311.

Cristini, V.; Tan, Y.-C. (2004): Theory and numerical simulation of droplet dynamics in complex flows - review. *Lab Chip*, vol. 4(4), pp. 257–264.

Eggers, J. (1995): Theory of drop formation. *Phys. Fluids*, vol. 7, pp. 941–953.

Eggers, J.; Dupont, T. (1994): Drop formation in a one-dimensional approximation of the Navier-Stokes equation. *J. Fluid Mech.*, vol. 262, pp. 205–221.

Eggleton, C. D.; Pawar, Y. P.; Stebe, K. J. (1999): Insoluble surfactants on a drop in an extensional flow: a generalization of the stagnated surface limit to deforming interfaces. *J. Fluid Mech.*, vol. 385, pp. 79–99.

Eggleton, C. D.; Tsai, T. M.; Stebe, K. J. (2001): Tip streaming from a drop in the presence of surfactants. *Phys. Rev. Lett.*, vol. 87(4), pp. 048302.

Esmaeeli, A. (2005): Phase distribution of bubbly flows under terrestrial and microgravity conditions. *Fluid Dyn. Mater. Process.*, vol. 1(1), pp. 63–80.

Ginzburg, I.; Wittum, G. (2001): Two-phase flows on interface refined grids modeled with vof, staggered finite volumes, and spline interpolants. *J. Comp. Phys.*, vol. 166, pp. 302–335.

Grace, H. P. (1982): Dispersion phenomena in high viscosity immiscible fluid systems and application of static mixers as dispersion devices in such systems. *Chem. Eng. Commun.*, vol. 14, pp. 225–277.

Guido, S.; Greco, F. (2004): Dynamics of a liquid drop in a flowing immiscible liquid. In Binding, D. M.; Walters, K.(Eds): *Rheology Reviews 2004*, pp. 99–142. British Society of Rheology.

Guido, S.; Simeone, M.; Greco, F. (2003): Deformation of a Newtonian drop in a viscoelastic matrix under steady shear flow. Experimental validation of slow flow theory. *J. Non-Newtonian Fluid Mech.*, vol. 114, pp. 65–82.

Hogea, C. S.; Murray, B. T.; Sethian, J. A. (2005): Implementation of the level set method for continuum mechanics based tumor growth models. *Fluid Dyn. Mater. Process.*, vol. 1(2), pp. 109–130.

Hooper, R.; Cristini, V.; Shakya, S.; Lowengrub, J. S.; Macosko, C. W.; Derby, J. J. (2001): Modeling multiphase flows using a novel 3d adaptive remeshing algorithm. In *Computational Methods in Multiphase Flow, Advances in Fluid Mechanics*, volume 29, pg. 10 pgs. Wessex Institute of Technology Press UK.

Hooper, R. W.; de Almeida, V. F.; Macosko, C. W.; Derby, J. J. (2001): Transient polymeric drop extension and retraction in uniaxial extensional flows. *J. Non-Newtonian Fluid Mech.*, vol. 98, pp. 141–168.

Hou, T. Y.; Lowengrub, J. S.; Shelley, M. J. (1997): The long-time motion of vortex sheets with surface tension. *Phys. Fluids*, vol. 9(7), pp. 1933–1954.

Hou, T. Y.; Lowengrub, J. S.; Shelley, M. J. (2001): Boundary integral methods for multicomponent fluids and multiphase materials. *J. Comp. Phys.*, vol. 169, pp. 302–362.

Jacqmin, D. (1999): Calculation of two-phase Navier-Stokes flows using phase-field modeling. *J. Comp. Phys.*, vol. 155, pp. 96–127.

Janssen, J. M. H. (1993): *Dynamics of liquid-liquid mixing*. PhD thesis, Tech. Univ. Eindhoven, 1993.

Jeong, J.; Dantzig, J.; Goldenfeld, N. (2003): Dendritic growth with fluid flow in pure materials. *Metall. Mater. Trans. A*, vol. 34, pp. 459–466.

Jeong, J.; Goldenfeld, N.; Dantzig, J. (2001): Phase field model for three-dimensional dendritic growth with fluid flow. *Phys. Rev. E*, vol. 64, pp. 041602–1 – 041602–14.

Jimenez, E.; Sussman, M.; Ohta, M. (2005): A computational study of bubble motion in Newtonian and viscoelastic fluids. *FDMP: Fluid Dyn. Mater. Process.*, vol. 1(2), pp. 97–108.

Keller, J.; Miksis, M. (1983): Surface tension driven flows. *SIAM J. Appl. Math.*, vol. 43, pp. 268–277.

Kennedy, M. R.; Pozrikidis, C.; Skalak, R. (1994): Motion and deformation of liquid drops and the rheology of dilute emulsions in simple flow. *Comput. & Fluids*, vol. 23, pp. 251–278.

Khismatullin, D.; Renardy, Y.; Cristini, V. (2003): Inertia-induced breakup of highly viscous drops subjected to simple shear. *Phys. Fluids*, vol. 15 (5), pp. 1351–1354.

Khismatullin, D.; Renardy, Y.; Cristini, V. (2006): Development and implementation of VOF-PROST for 3d viscoelastic liquid-liquid simulations. *J. Non-Newt. Fluid Mech.*

Kobayashi, I.; Yasuno, M.; Iwamoto, S.; Shono, A.; Satoh, K.; Nakajima, M. (2002): Microscopic observation of emulsion droplet formation from a polycarbonate membrane. *Colloids Surf.*, vol. 207, pp. 185–196.

Lappa, M. (2005): Coalescence and non-coalescence phenomena in multi-material problems and dispersed multiphase flows: Part 1, A critical review of theories. *FDMP: Fluid Dyn. Mater. Process.*, vol. 1 (3), pp. 201–212.

Lappa, M. (2005): Coalescence and non-coalescence phenomena in multi-material problems and dispersed multiphase flows: Part 2, A critical review of CFD approaches. *FDMP: Fluid Dyn. Mater. Process.*, vol. 1 (3), pp. 213–234.

Li, J.; Renardy, Y.; Renardy, M. (2000): Numerical simulation of breakup of a viscous drop in simple shear flow through a volume-of-fluid method. *Phys. Fluids*, vol. 12(2), pp. 269–282.

Li, X.; Pozrikidis, C. (1997): The effects of surfactants on drop deformation and on the rheology of dilute emulsions in Stokes flow. *J. Fluid Mech.*, vol. 341, pp. 165–194.

Lister, J. R.; Stone, H. A. (1998): Capillary breakup of a viscous thread surrounded by another viscous fluid. *Phys. Fluids*, vol. 10, pp. 2758–2764.

Lowengrub, J.; Goodman, J.; Lee, H.; Longmire, E.; Shelley, M.; Truskinovsky, L. (1999): Topological transitions in liquid/liquid interfaces. In Athanasopoulos, I.; Makrakis, M.; Rodrigues, J.(Eds): *Free boundary problems: theory and applications*, pp. 221–236. CRC Press, London.

Mabille, C.; Schmitt, V.; Gorria, P.; Calderon, F. L.; Faye, V.; Deminiére, B.; Bibette, J. (2000): Rheological and shearing conditions for the preparation of monodisperse emulsions. *Langmuir*, vol. 16, pp. 422–429.

Maldarelli, C.; Huang, W. (1996): The effect of surfactants on the motion of bubbles and drops. *Flow of Particles in Suspensions, Springer, New York*, vol. CISM Courses and Lectures No.370, pp. 125–160.

Mansour, N.; Lundgren, T. (1990): Satellite formation in capillary jet breakup. *Phys. Fluids A*, vol. 2, pp. 1141–1144.

Marks, C. R. (1998): *Drop breakup and deformation in sudden onset strong flows*. PhD thesis, University of Maryland at College Park, 1998.

Mason, T. G.; Bibette, J. (1997): Shear rupturing of droplets in complex fluids. *Langmuir*, vol. 13, pp. 4600–4613.

Mason, T. G.; Bibette, J.; Weitz, D. A. (1996): Yielding and flow of monodisperse emulsions. *J. Colloid Interface Sci.*, vol. 179, pp. 439.

Milliken, W. J.; Leal, L. G. (1994): The influence of surfactant on the deformation and breakup of a viscous drop – the effect of surfactant solubility. *J. Colloid Interface Sci.*, vol. 166, pp. 275.

Milliken, W. J.; Stone, H. A.; Leal, L. G. (1993): The effect of surfactant on the transient motion of newtonian drops. *Phys. Fluids A*, vol. 5(1), pp. 69–79.

Navot, Y. (1999): Critical behavior of drop breakup in axisymmetric viscous flow. *Phys. Fluids*, vol. 11, pp. 990–996.

Nobari, M.; Jan, Y.-J.; Tryggvason, G. (1996): Head-on collision of drops–a numerical investigation. *Phys Fluids*, vol. 8, pp. 29–42.

Notz, P. K.; Chen, A. U.; Basaran, O. A. (2001): Satellite drops: unexpected dynamics and change of scaling during pinch-off. *Phys. Fluids*, vol. 13(3), pp. 549–552.

Nourgaliev, R. R.; Dinh, T. N.; Theofanous, T. G.; Joseph, D. (2003): The Lattice Boltzmann equation method: Theoretical interpretation, numerics and implications. *Intern. J. Multiphase Flows*, vol. 29, pp. 117–169.

Osher, S.; Fedkiw, R. (2001): Level set methods: an overview and some recent results. *J. Comp. Phys.*, vol. 169, pp. 463–502.

Papageorgiou, D. T. (1995): On the breakup of viscous liquid threads. *Phys. Fluids*, vol. 7, pp. 1529–1544.

Pawar, Y. P.; Stebe, K. J. (1996): Marangoni effects on drop deformation in an extensional flow: The role of surfactant physical chemistry. i. insoluble surfactants. *Phys. Fluids*, vol. 8(7), pp. 1738–1751.

Pozrikidis, C. (1992): *Boundary integral and singularity methods for linearized viscous flow*. Camb. Univ. Press.

Pozrikidis, C. (2002): Expansion of a two-dimensional foam. *Eng. Annal. Bound. Elem.*, vol. 26, pp. 495–504.

Prosperetti, A.; Oguz, H. (1997): Air entrainment upon liquid impact. *Phil. Trans. R. Soc. Lond. A*, vol. 355, pp. 491–506.

Provatas, N.; Goldenfeld, N.; Dantzig, J. (1999): Adaptive mesh refinement computation of solidification microstructures using dynamic data structures. *J. Comp. Phys.*, vol. 148, pp. 265.

Rallison, J. M. (1981): A numerical study of the deformation and burst of a drop in general shear flows. *J. Fluid Mech.*, vol. 109, pp. 465–482.

Rallison, J. M. (1984): The deformation of small viscous drops and bubbles in shear flows. *Ann. Rev. Fluid Mech.*, vol. 16, pp. 45–66.

Renardy, Y.; Cristini, V. (2001): Effect of inertia on drop breakup under shear. *Phys. Fluids*, vol. 13(1), pp. 7–13.

Renardy, Y.; Cristini, V. (2001): Scalings for fragments produced from drop breakup in shear flow with inertia. *Phys. Fluids*, vol. 13(8), pp. 2161–2164.

Renardy, Y.; Cristini, V.; Li, J. (2002): Drop fragment distributions under shear with inertia. *Int. J. Mult. Flow*, vol. 28, pp. 1125–1147.

Renardy, Y.; Renardy, M. (2002): PROST: a parabolic reconstruction of surface tension for the volume-of-fluid method. *J. Comp. Phys.*, vol. 183(2), pp. 400–421.

Rothman, D. H.; Zaleski, S. (1997): *Lattice Gas Cellular Automata*. Cambridge University Press.

Sankaranarayanan, K.; Kevrekidis, I.; Sundaresan, S.; Lu, J.; Tryggvason, G. (2003): A comparative study of lattice Boltzmann and front-tracking finite-difference methods for bubble simulations. *Int. J. Multiphase Flows*, vol. 29, pp. 109–116.

Scardovelli, R.; Zaleski, S. (1999): Direct numerical simulation of free surface and interfacial flow. *Ann. Rev. Fluid Mech.*, vol. 31, pp. 567–604.

Schmitt, V.; Leal-Calderon, F.; Bibette, J. (2003): Preparation of monodisperse particles and emulsions by controlled shear. In *Colloid Chem. II. Book series: topics in current chemistry*, volume 227, pp. 195–215. Springer-Verlag Berlin.

Shin, S.; Juric, D. (2002): Modeling three-dimensional multiphase flow using a level contour reconstruction method for front tracking without connectivity. *J. Comp. Phys.*, vol. 180, pp. 427–470.

Siegel, M. (1999): Influence of surfactant on rounded and pointed bubbles in 2D Stokes flow. *SIAM J. Appl. Math*, vol. 59(6), pp. 1998–2027.

Stone, H. A. (1994): Dynamics of drop deformation and breakup in viscous fluids. *Ann. Rev. Fluid Mech.*, vol. 26, pp. 65–102.

Stone, H. A.; Leal, L. G. (1989): Relaxation and breakup in an initially extended drop in an otherwise quiescent fluid. *J. Fluid Mech.*, vol. 198, pp. 399–427.

Stone, H. A.; Leal, L. G. (1990): The effects of surfactants on drop deformation and breakup. *J. Fluid Mech.*, vol. 220, pp. 161–186.

Sussman, M.; Almgren, A. S.; Bell, J. B.; Colella, P.; Howell, L. H.; Welcome, M. L. (1999): An adaptive level set approach for imcompressible two-phase flows. *J. Comp. Phys.*, vol. 148(1), pp. 81–124.

Sussman, M.; Puckett, E. G. (2000): A coupled level set and volume-of-fluid method for computing 3D and axisymmetric incompressible two-phase flows. *J. Comput. Phys*, vol. 162(2), pp. 301–337.

Tan, Y. C.; Cristini, V.; Lee, A. P. (2006): Monodispersed microfluidic droplet generation by shear focusing

microfluidic device. *Sensors and Actuators B*, vol. in press.

Tjahjadi, M.; Stone, H. A.; Ottino, J. M. (1992): Satellite and subsatellite formation in capillary breakup. *J. Fluid Mech.*, vol. 243, pp. 297–317.

Tryggvason, G.; Bunner, B.; Esmaeeli, A.; Juric, D.; Al-Rawahi, N.; Tauber, W.; Han, J.; Nas, S.; Jan, Y.-J. (2001): A front-tracking method for the computations of multiphase flow. *J. Comp. Phys.*, vol. 169, pp. 708–759.

Ubbink, O.; Issa, R. (1999): A method for capturing sharp fluid interfaces on arbitrary meshes. *J. Comp. Phys.*, vol. 153, pp. 26–50.

Umbanhowar, P. B.; Prasad, V.; Weitz, D. A. (2000): Monodisperse emulsion generation via drop break off in a coflowing stream. *Langmuir*, vol. 16, pp. 347–351.

Utracki, L. A.; Shi, Z. H. (1992): Development of polymer blend morphology during compounding in a twin-screw extruder. Part I: droplet dispersion and co-alescence - a review. Part II: Theoretical derivations. Part III: experimental procedure and preliminary results. *Polymer Eng. Sci.*, vol. 32:24, pp. 1824–1856.

Watanabe, T.; Ebihara, K. (2003): Numerical simulation of coalescence and breakup of rising droplets. *Comput. Fluids*, vol. 32, pp. 823–834.

Wilkes, E. D.; Phillips, S. D.; Basaran, O. A. (1999): Computational and experimental analysis of dynamics of drop formation. *Phys. Fluids*, vol. 11(12), pp. 3577–3598.

Yabe, T.; Xiao, F.; Utsumi, T. (2001): The constrained interpolation profile method for multiphase analysis. *J. Comp. Phys.*, vol. 169, pp. 556–593.

Yeo, L. Y.; Matar, O. K.; de Ortiz, E. S. P.; Hewitt, G. E. (2003): Film drainage between two surfactant-coated drops colliding at constant approach velocity. *J. Coll. Int. Sci.*, vol. 257, pp. 93–107.

Yue, P.; Feng, J. J.; Liu, C.; Shen, J. (2004): A diffuse-interface method for simulating two-phase flows of complex fluids. *J. Fluid Mech.*, vol. 515, pp. 293–317.

Yue, P.; Feng, J. J.; Liu, C.; Shen, J. (2005): Viscoelastic effects on drop deformation in steady shear. *J. Fluid Mech.*, vol. 540, pp. 427 – 437.

Zhao, X.; Goveas, J. L. (2001): Size selection in viscoelastic emulsions under shear. *Langmuir*, vol. 17, pp. 3788–3791.

Zheng, B.; Roach, L. S.; Ismagilov, R. F. (2003): Screening of protein crystallization conditions on a microfluidic chip using nanoliter-size droplets. *J. Am. Chem. Soc.*, vol. 125, pp. 11170–11171.

Zheng, X.; Lowengrub, J.; Anderson, A.; Cristini, V. (2005): Adaptive unstructured mesh -II. Application to two- and three-dimensional level-set simulations of multiphase flow. *J. Comp. Phys.*, vol. 208, pp. 626–650.

Zinchenko, A. Z.; Rother, M. A.; Davis, R. H. (1999): Cusping, capture and breakup of interacting drops by curvatureless boundary-integral algorithm. *J. Fluid Mech.*, vol. 391, pp. 249–292.